Submitted: 25 May, 2023 Accepted: 28 June, 2023 Published: 15 December, 2024 DOI:10.22514/ejgo.2024.116

ORIGINAL RESEARCH

European Journal of Gynaecological Oncology

Necroptosis-related gene to construct a signature to predict the prognosis and immune features in patients with cervical cancer

Yongming Du[1], Yichao Hu[2], Mengmeng Qiu[3], Yuehua Sheng[1,*]

[1]Department of Gynecology and Obstetrics, The First Affiliated Hospital of Ningbo University, 315000 Ningbo, Zhejiang, China
[2]Department of Urology, The First Affiliated Hospital of Ningbo University, 315000 Ningbo, Zhejiang, China
[3]Department of Oncology, Ningbo Chinese Medical Hospital, 315000 Ningbo, Zhejiang, China

***Correspondence**
shengyuehua@nbdyyy.com
(Yuehua Sheng)

Abstract

Cervical cancer (CC) is the fourth most deadly disease in women. Necroptosis is a programmed form of necrosis. Increasing evidences indicated that abnormal expression of necroptosis-related genes was associated with prognosis in cancers. However, the value of necroptosis-related genes (NRGs) as potential prognostic biomarker for CC is still unclear. The expression matrix and clinicopathological information were achieved from the The Cancer Genome Atlas (TCGA) and The Genotype-Tissue Expression (GTEx) datasets. Consensus clustering classification was performed and its correlation with prognosis, clinicopathological features and immunity was analyzed. Subsequently, we constructed a risk signature (NRGscore) by least absolute shrinkage and selection operator (LASSO) regression analysis. CIBERSORT, single sample geneset enrichment analysis (ssGSEA) and ESTIMATE were used to explore the difference in immune landscape in patients with different risks. We also evaluated the NRGscore signature in immunotherapy and chemotherapy response prediction between high- and low-risk groups. Quantitative reverse transcription PCR (qRT-PCR) was performed to validate the expression difference of key genes in CC tissues. We constructed the prognostic signature with 9 necroptosis-related genes and patients with high-risk score featured with significantly worse prognosis, lower proportion of immune cell infiltration, and higher proportion of immunosuppressive cells. Multivariate regression analyses displayed that NRGscore signature could not only independently predicted the overall survival but also performed better than any other clinical and pathological factors. The qRT-PCR results demonstrated most of NRGs were differently expressed in CC samples. The NRGscore signature effectively predicted the prognosis of CC patients and demonstrated close relationship with the tumor immune microenvironment, chemotherapy and immunotherapy responses. These NRGs could provide potential targets with regard to the immunotherapy for individualized treatment.

Keywords

Cervical cancer; Chemotherapy; Necroptosis; Immunotherapy; Prognosis

1. Introduction

Cervical cancer (CC) is the fourth most common malignancy in women, with over 600,000 new cases projected globally in 2020 [1]. Most CC (over 95%) is caused by persistent human papillomavirus (HPV) infection, particularly HPV 16 and 18. Vaccination against HPV, along with screening tests such as Pap smears and HPV tests, are effective in preventing CC. Early-stage CC may present with nonspecific clinical symptoms, and as the tumor progresses, more severe symptoms develop. Treatment options include surgery, radiotherapy, chemotherapy and immunotherapy. Despite intensive therapy, the recurrence rates in patients with advanced stages can reach nearly 70% [2, 3]. Despite intensive therapy, the treatment of recurrent CC remains clinically challenging and is associated with worst prognosis [4]. Therefore, there is an urgent need for reliable biomarkers and the development of innovative prognostic signatures for CC to improve the treatment outcomes of these patients.

Necroptosis is a specific form of programmed cell death that plays important roles in physiological and pathological processes [5]. Recent studies have shown that changes in necroptosis are closely related to the occurrence and development of cancer. In many types of tumors, inhibition or loss of the necroptosis pathway can lead to proliferation and drug resistance of tumor cells, thereby promoting tumor progression and metastasis [6–10]. Several studies have demonstrated the importance of necroptosis-related genes in various cancers. For example, different expression levels of genes such as receptor-interacting protein kinase 1 (*RIPK1*), receptor-

interacting protein kinase 3 (*RIPK3*) and mixed lineage kinase domain-like (*MLKL*) are closely related to the occurrence and prognosis of multiple cancers [11–13]. In addition, the mechanisms of action of many anti-tumor drugs are also related to the regulation of the necroptosis pathway [14, 15]. Therefore, in-depth research and analysis of necroptosis-related genes can help us better understand the mechanisms of tumor occurrence, development and treatment, and provide a theoretical basis for the development of new tumor treatment strategies. However, necroptosis-related genes (NRGs) as a possible prognostic biomarker for CC remains undetermined.

Herein, we established a novel NRGs signature for predicting the prognosis of patients with CC through data mining of The Cancer Genome Atlas (TCGA) dataset. The overall design and technical flowchart of the study are presented in Fig. 1. By analyzing the mRNA expression profiles and clinical data of CC patients, we successfully identify differentially expressed genes (DEGs) with prognostic significance related to the NRGs. Then, we establish an NRGs signature using the least absolute shrinkage and selection operator (LASSO) regression analysis and validate its predictive performance using the Gene Expression Omnibus (GEO) validation datasets. Additionally, we perform enrichment and immune infiltration analysis on the DEGs from the high- and low-risk groups. The results demonstrate a strong correlation between the novel prognostic signature, tumor microenvironment (TME) and chemotherapy and immunotherapy responses, suggesting its promising prognostic value and potential utility in guiding individualized chemotherapy and immunotherapeutic in CC patients. Furthermore, we verify the mRNA and protein expression levels of nine key NRGs in CC patients' tissues using qRT-PCR.

2. Methods

2.1 Data download and process

A total of 159 genes from the necroptosis pathway were extracted from the Kyoto Encyclopedia of Genes and Genomes (KEGG) database. The expression matrix and clinical data of CC patients were obtained from the TCGA dataset, and the expression profiles of normal cervical samples were obtained from the Genotype-Tissue Expression database. To validate the robustness of our gene signature, microarray data and related clinical characteristics were retrieved from GEO datasets, including GSE30760, GSE52903 and GSE44001. Then these expression profile data were normalized to remove batch effects and for further analysis. Only patients with histological confirmation of CC and available survival information were included in this study.

2.2 Expression levels of NRGs in CC

From the TCGA-CESC cohort and GTEx database, a total of 12,273 differentially expressed genes (DEGs) were identified using the "DESeq2" package (version 1.40.2) using a threshold of $p < 0.05$ and the $|\text{LogFC}| > 1$. Additionally, 159 previously published NRGs were included, among which 51 NRGs showed differential expression and were used to construct a protein-protein interaction network using the STRING database and visualized through Cytoscape. Furthermore, NRGs correlated with prognosis were identified by performing univariate Cox regression analysis using the "tinyarray" package (version 2.2.7).

2.3 Consensus clustering analysis for NRGs

To identify distinct patterns related to necroptosis, consensus unsupervised clustering analysis was performed using the k-means clustering method with the "ConsensusClusterPlus" package (version 1.54.0) and a maximum evaluated k value of 9 and 1000 resamplings. The optimal value of k was determined based on the relative increase in consensus and the point where there was no significant further increase. Subsequently, patients were assigned to the defined clusters and a comparison was made among the clusters in terms of clinicopathological features, prognosis, tumor microenvironment (TME), and immune responses.

2.4 Establishment and evaluation of NRGs signature

We used LASSO analysis to obtain the necroptosis regulators correlating with prognosis and the corresponding regression coefficients. Based on the LASSO regression results, an NRGs gene signature (NRGscore) was developed for the investigated CC patients, whose risk score was calculated using the following formula: $\sum_{i=1}^{n} Coef_i \times X_i$, where $Coef_i$ refers to the expression data of each necroptosis regulator. After categorizing patients into high- and low-risk subgroups based on the median risk score, we conducted Kaplan-Meier (KM) analysis using the "tinyarray" package to compare the overall survival rates between these groups. Additionally, the accuracy of the NRGscore signature was assessed using receiver operating characteristic (ROC) curves. Time-independent ROC analyses were performed to evaluate the predictive accuracy of the NRGscore signature for 1-, 3- and 5-year survival. The area under the curves (AUCs) were used to measure the prognostic accuracy and compared with clinicopathological characteristics to assess predictive performance. Principal Component Analysis (PCA) and t-distributed Stochastic Neighbor Embedding (tSNE) were utilized for dimension reduction and visualization of patient diversity between comparison groups. To determine if the NRGscore signature can be applied to patients with different clinicopathological stratifications, CC patients were divided into comparison groups based on factors such as age, grade and international federation of gynecology and obstetrics (FIGO) stage, then their overall survival rates for the high- and low-risk patients were compared using KM analysis.

Next, the external datasets GSE30760, GSE52903 and GSE44001 were used to evaluate the predictive performance of this NRGscore signature. Then, these microarray data and corresponding clinical information were extracted from the GEO database using the "GEOquery" software (version 2.58.0). **Supplementary Table 1** presents the baseline characteristics of the CC patients from the TCGA and GEO datasets.

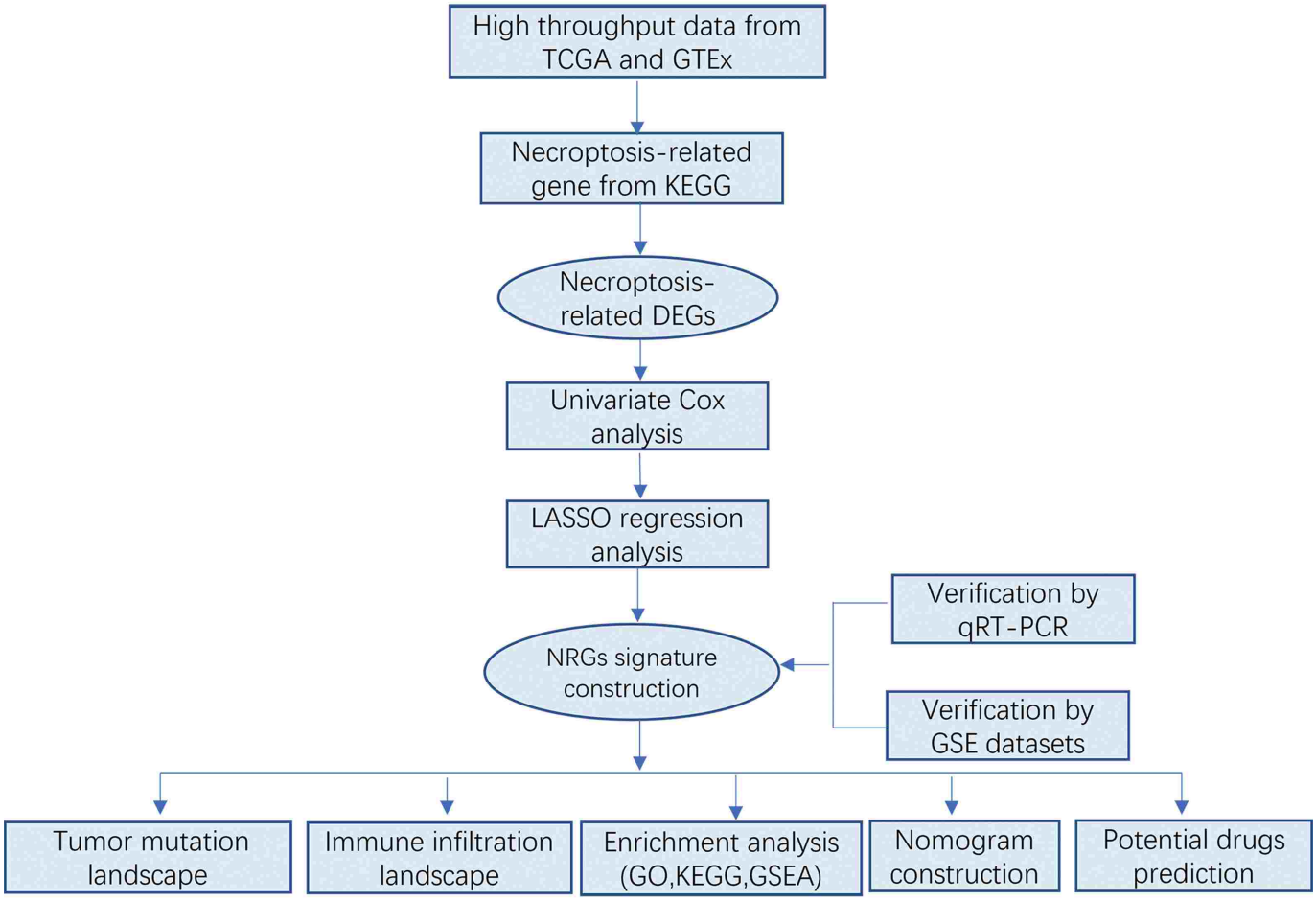

FIGURE 1. The study's flow chart. TCGA, The Cancer Genome Atlas; GTEx, The Genotype-Tissue Expression; KEGG, Kyoto Encyclopedia of Genes and Genomes; DEGs, differentially expressed genes; LASSO, least absolute shrinkage and selection operator; qRT-PCR, quantitative reverse transcription PCR; GEO, Gene Expression Omnibus; NRGs, necroptosis-related genes; GO, Gene Ontology; GSEA, Gene set enrichment analysis.

2.5 Functional enrichment analysis

Gene set enrichment analysis (GSEA) was performed to determine the potential underlying regulatory mechanisms using the gene set "c2.cp.kegg.v7.4.symbols.gmt" obtained from the Broad Institute database. Gene Ontology (GO) and KEGG functional enrichment were also conducted, and all these analyses were performed using the R packages "limma", "clusterProfiler", "gseaplot2" and "ggplot2".

2.6 Mutation spectrum analyses

Tumor mutation burden (TMB) was used to predict the effect of immunotherapeutic response. Additionally, waterfall plots were drawn to display the mutation landscape using the "maftools" package (version 2.6.05). Furthermore, the association between TMB and risk score was evaluated using Pearson correlation analysis, with statistical significance set at $p < 0.05$.

2.7 Tumor microenvironment cell infiltration analyses

The CIBERSORT deconvolution algorithm was used to evaluate the immune infiltration proportion of 22 immune cell subtypes based on gene expression values. The patients were categorized into distinct proportion groups based on their immune cell infiltration level, and their overall survival rate difference was compared using the KM survival analysis. Pearson correlation analysis was performed to determine the relationship between the degree of immune cell infiltration and the risk ratings. Additionally, ssGSEA was used to assess the percentage of immune cells infiltrating a tissue and the potential immunological activities.

2.8 Immunotherapy response prediction

To assess the difference in immunogenicity between the comparison groups, we collected information on immunophenoscore (IPS) from The Cancer Imaging Archive database for patients with CC. IPS is a numerical score ranging from 0 to 10, which reflects the level of immunogenicity based on four key gene categories, where a higher IPS score indicates greater immunogenicity. IPS is a potential marker for predicting the response to cytotoxic T-lymphocyte-associated protein 4 (CTLA-4) and programmed death ligand 1 (PD-L1) antibodies. Tumor immune dysfunction and exclusion (TIDE) scores were calculated using a normalized corrected expression matrix obtained from the TIDE database. Patients

with lower TIDE scores are more likely to exhibit improved responses and increased sensitivity to immune checkpoint inhibitors (ICIs). To assess the correlation between immune checkpoint genes and the NRGscore model, we analyzed the expression matrix of immune checkpoint genes in both high- and low-risk categories. Additionally, we examined the relationship between the risk score and immune checkpoint genes using the "ggplot2" software (version 3.4.0). The immune cytolytic activity score (CYT) is a novel biomarker for antitumor immunity, which is calculated as the geometric mean of perforin (PRF1) and granzyme A (GZMA) mRNA expression levels. PRF1 and GZMA are significantly upregulated during $CD8^+$ T cell activation and in clinical responses to CTLA4 or PD-L1 antibody treatments, and their upregulation has also been associated with improved patient survival.

2.9 Analysis of potential chemotherapy drugs and compounds

We utilized the Genomics of Drug Sensitivity in Cancer (GDSC) database to predict chemotherapeutic sensitivity, specifically by calculating the half maximal inhibitory concentration (IC50). Furthermore, we employed the "DESeq2" method to identify DEGs between the high- and low-risk subgroups; then, the potential anti-cancer compounds were assessed in the Connectivity Map (CMap) database (https://clue.io/).

2.10 Total RNA extraction and real-time quantitative PCR (qRT-PCR)

The CC and adjacent non-tumor samples were obtained from the Department of Gynecology at Ningbo First Hospital. Total RNA was extracted from the cervical tissues using the TRIzol reagent (10296028, Invitrogen, Carlsbad, CA, USA) following the manufacturer's instructions. Then, cDNAs were generated using the SuperScript III Reverse Transcriptase kit (11752050, ABI-Invitrogen, Carlsbad, CA, USA) and subjected to qRT-PCR analysis using the SYBR qPCR Mix (4472920, ABI-invitrogen, Carlsbad, CA, USA) on the StepOnePlus Real-Time PCR system (Applied Biosystems, USA). The primer sequences used for the analysis are shown in Table 1. The Human Protein Atlas (HPA) database, which integrates multiple omics technologies to map human proteins in cells, tissues and organs, was searched to identify representative images of immunohistochemistry displaying the expression of hub NRGs.

2.11 Statistical analyses

Statistical significance between comparison groups was evaluated using both the two-sample *t*-test and the Wilcoxon-Mann-Whitney test. The survival analysis of different risk score subgroups was performed using the KM method with the "survminer" and "survival" packages. The statistical analyses were conducted using R software (version 4.0.4, University of Auckland, Auckland, New Zealand).

3. Results

3.1 Analyses of differentially expressed NRGs in CC

Firstly, we integrated expression matrix of 303 cancer tissues from the TCGA-CESC dataset and ten normal tissues from the GTEx database and identified 12,273 DEGs. Then, we isolated the expression values of 51 differentially expressed NRGs. Among these DEGs, glycogen phosphorylase, muscle associated (*PYGM*), (*MAPK10*), calcium/calmodulin dependent protein kinase ii alpha (*CAMK2A*), BCL2 apoptosis regulator (*BCL2*), jumonji domain containing 7-phospholipase a2, group ivb (cytosolic) read-through (*JMJD7-PLA2G4B*), signal transducer and activator of transcription 5b (*STAT5B*), phospholipase a2 group ivb (*PLA2G4B*), TNF Receptor Associated Factor 5 (*TRAF5*) and toll like receptor 4 (*TLR4*) were downregulated in tumor samples, the rest of NRGs were all upregulated. To further investigate the connection among these NRGs, we utilized STRING database to develop protein-protein interaction (PPI) network. Using the CytoHubba plugin and MCC algorithm, we identified the top 35 shared genes (**Supplementary Fig. 1A**). Furthermore, to explore the corre-

TABLE 1. Primer sequences for real-time quantitative PCR.

Gene	Forward primer (5′-3′)	Reverse primer (5′-3′)
IL-1β	TTTGAGTCTGCCCAGTTCCC	GTTATATCCTGGCCGCCTT
H2AZ1	TGAACTGGCAGGAAATGCATC	CCACCAGCAATTGTAGCCTT
H2AC14	GTACCTGACCGCCGAGATCCT	GCTCCTCATCGTTGCGGATGG
TNFAIP3	CGCCTGTGATCATTTTGGCAAT	AGCCATACATCTGCTTGAACTGA
CHMP4C	TGGGCAAGAAACAAGAGTACCTG	CCTCTTCTTTCTCTTTAGTGCCT
PLA2G4B	CTACTGTGCCCTCAACACCAA	GCTGCCCCATAAAGAACTCGGA
BCL2	GAGGAGCTTTGTTTCAACCA	AATACCATGAATTAAATGCGGAA
CYBB	ATTCTCTTGCCAGTCTGTCG	TGAAGTGCAATCATCCATGCC
SLC25A5	CTGTTGCCGGGTTGACTTCC	GCCTCCTTCATCACGAGCAAT

IL-1β, interleukin-1β; H2AZ1, H2A.Z variant histone 1; H2AC14, H2A clustered histone 14; TNFAIP3, TNF alpha induced protein 3; CHMP4C, charged multivesicular body protein 4c; PLA2G4B, phospholipase a2 group ivb; BCL2, BCL2 apoptosis regulator; CYBB, cytochrome b-245 beta chain; SLC25A5, solute carrier family 25 member 5.

lation among these NRGs, we carried out Pearson correlation analysis on these 51 genes (**Supplementary Fig. 1B**). The results demonstrated that fas ligand (*FASLG*), *IL-1β, PLA2G4B* and pyd and card domain containing (*PYCARD*) displayed strong positive correlations with Interferon Gamma (*IFNG*) (cor = 0.86), interleukin 1 alpha (*IL1A*) (cor = 0.85), JMJD7-PLA2G4B (cor = 0.79) and charged multivesicular body protein 2a (*CHMP2A*) (cor = 0.67) respectively. While peptidylprolyl isomerase a (*PPIA*) and *CHMP2A* were negatively correlated with the *TRAF5* (cor = −0.32) and *TNFRSF10A* (cor = −0.34). These results indicated that necroptosis-related genes may play a crucial part in the initiation and development of CC carcinogenesis.

3.2 Identification of prognostic NGRs and consensus clustering analysis

After integrating the clinical information with the expression matrix of 303 tumor samples, we performed univariate Cox regression analysis on the 51 NRGs, using a selection criterion of $p < 0.05$, to identify prognostic genes for CC. Eleven NRGs showing potential prognostic value for CC were identified, namely five risky genes (*CHMP4C*, *TNFAIP3*, *IL1A*, fas associated *via* death domain (*FADD*) and *IL-1β*) and six protective genes (*H2AC14*, *SLC25A5*, *CYBB*, *H2AZ1*, *PLA2G4B* and *BCL2*). Using consensus clustering analysis, the optimal value of k was determined to be 3, which was used to assign patients into three distinct clusters (Fig. 2A). ClusterA consisted of 153 cases, ClusterB had 97 cases, and ClusterC included 25 cases. Hierarchical clustering revealed distinct expression patterns of five NRGs among the three clusters (**Supplementary Fig. 2**). Furthermore, KM survival analysis showed significant differences in overall survival rates among the three clusters (Fig. 2B), with patients from ClusterA demonstrating the worst prognosis. Additionally, we compared the clinical characteristics among the three clusters, and the results indicated that patients from ClusterA had more severe clinical symptoms than those in ClusterB and ClusterC. Fig. 2C illustrates the different clinicopathological features observed in the three clusters.

3.3 Immune cell infiltration patterns in different clusters

To investigate the TME in different clusters, we evaluated the percentage of immune cell infiltration using ssGSEA, which revealed different clusters displaying distinct immune cell infiltration (Fig. 3A). ClusterC exhibited a high proportion of B cells, macrophages, neutrophils and tumor-infiltrating lymphocytes (TILs). ClusterB showed a lower proportion of immune cell infiltration compared to ClusterC. ClusterA had a low proportion of immune cells and only showed a high proportion of neutrophils and TILs. Furthermore, we assessed the average immune score, estimate score and stromal score, which were higher in ClusterC than ClusterA and ClusterB. Additionally, the tumor purity in ClusterC was the lowest among the three clusters (Fig. 3B). Moreover, no significant difference was observed upon comparing the expression levels of human leukocyte antigen (HLA) genes, TMB levels and IPS analyses among the three clusters (**Supplementary Fig. 3**).

3.4 Construction of the NRGs signature

To establish the NRGscore, we used the LASSO regression algorithm to analyze the eleven NRGs (Fig. 4A,B). The signature comprised nine necroptosis-related genes: *H2AZ1*, *H2AC14*, *PLA2G4B*, *BCL2*, *CYBB* and *SLC25A5*, which were downregulated (coefficients <0), were considered protective genes, while *IL1B*, *TNFAIP3* and *CHMP4C*, which were upregulated (coefficients >0), were considered risky genes. The risk score calculation is as follows: Risk score = (0.019 × *IL1B* expression value) + (−0.001 × *H2AZ1* expression value) + (−0.172 × *H2AC14* expression value) + (0.009 × *TNFAIP3* expression value) + (0.045 × *CHMP4C* expression value) + (−0.027 × *PLA2G4B* expression value) + (−0.096 × *BCL2* expression value) + (−0.021 × *CYBB* expression value) + (−0.001 × *SLC25A5* expression value). Based on the median risk score, the CC patients were divided into a high-risk subgroup (n = 137 patients) and a low-risk subgroup (n = 138 patients). Then, PCA and tSNE were used for dimension reduction and to visualize the diversity. The results demonstrated that the high-risk and low-risk patients could be well-demarcated (Fig. 4F,G).

3.5 Validation of the NRGscore signature

To validate the robustness of the NRGscore signature, we integrated the expression matrix of *IL1B*, *TNFAIP3*, *CHMP4C*, *PLA2G4B*, *BCL2*, *CYBB* and *SLC25A5*, along with the corresponding survival information from the GSE30760, GSE52903 and GSE44001 datasets. Then, the risk scores for the samples in these datasets were calculated using the above-mentioned formula. The validation results exhibited strong agreement with those obtained from the TCGA cohort, with CC patients with higher risk scores demonstrating worse prognoses ($p < 0.001$) (**Supplementary Fig. 4C**). The survival status and risk score distributions are shown in **Supplementary Fig. 4A,B**, respectively. Furthermore, the ROC curves demonstrate the superior predictive ability of our signature for CC patients (**Supplementary Fig. 4D**). Collectively, these findings provide evidence that our NRGscore signature exhibits good prognostic performance in CC.

3.6 Association of risk score model with the prognosis of CC patients

To evaluate the predictive performance of the NRGscore model, KM curves were generated to compare the prognosis between different risk score groups. The results indicated that CC patients with low risk scores had a significantly better prognosis ($p < 0.001$; Fig. 4D). The survival status and risk score distributions are illustrated in Fig. 4C,E, respectively, which shows that as the risk scores increased, a larger number of CC patients experienced unfavorable outcomes. Univariate analysis demonstrated a significant correlation between the risk score and prognosis (hazard ratio (HR): 3.030, 95% confidence interval (CI): 1.990–4.137, $p < 0.001$; Fig. 4H). Furthermore, multivariate analysis confirmed that the NRGscore signature independently predicted prognosis (HR: 2.870, 95% CI: 1.851–4.448, $p < 0.001$; Fig. 4I).

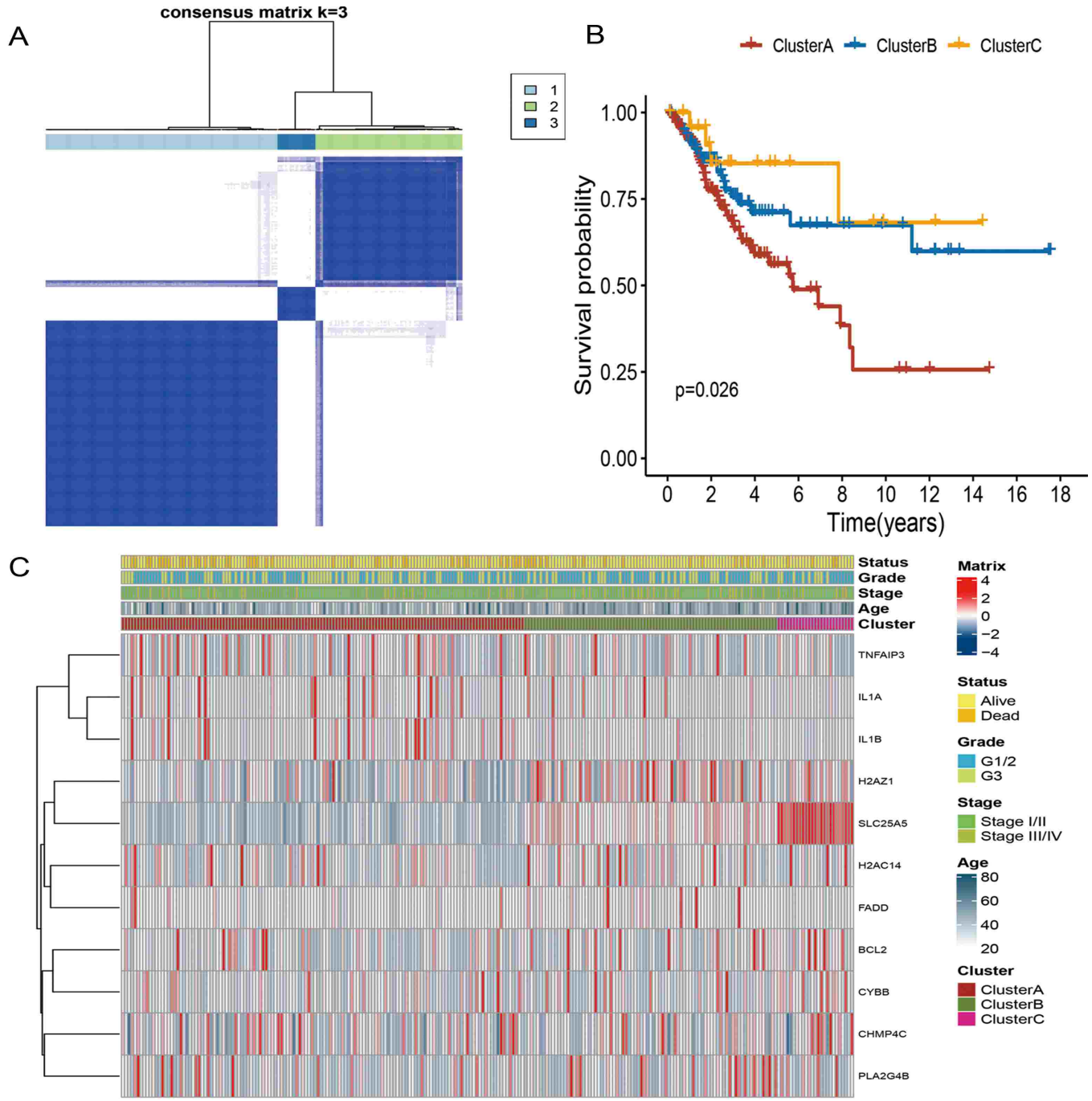

FIGURE 2. Consensus clustering analysis, stratification of clinicopathological characterization, and prognosis difference of the three clusters in cervical cancer. (A) k = 2 was used to ensure the clustering stability. (B) Survival analysis for the distinct clusters using Kaplan-Meier curves. (C) The different clinicopathological features of the three clusters. G1/2, Grade 1/2; G3, Grade 3.

ROC curve analysis demonstrated that our gene signature outperformed other clinical and pathological criteria. The AUC values for 1, 3 and 5-year survival were 0.708, 0.685 and 0.765, respectively, indicating a good prognostic ability (Fig. 4J).

3.7 Stratification analyses of the NRGscore signature in clinicopathological features

To evaluate whether the NRGscore signature can be applied to CC patients with different clinical stratifications, we divided them into comparison groups based on age, grade and FIGO stage and compared their overall survival time *via* KM analyses. The results demonstrated that the NRGscore characteristics could effectively predict the prognosis of CC patients across different clinical categories (**Supplementary Fig. 5**).

3.8 Construction of the NRGscore signature-based nomogram

We constructed a nomogram that serves as a clinically applicable tool to predict the overall survival (OS) time of CC patients

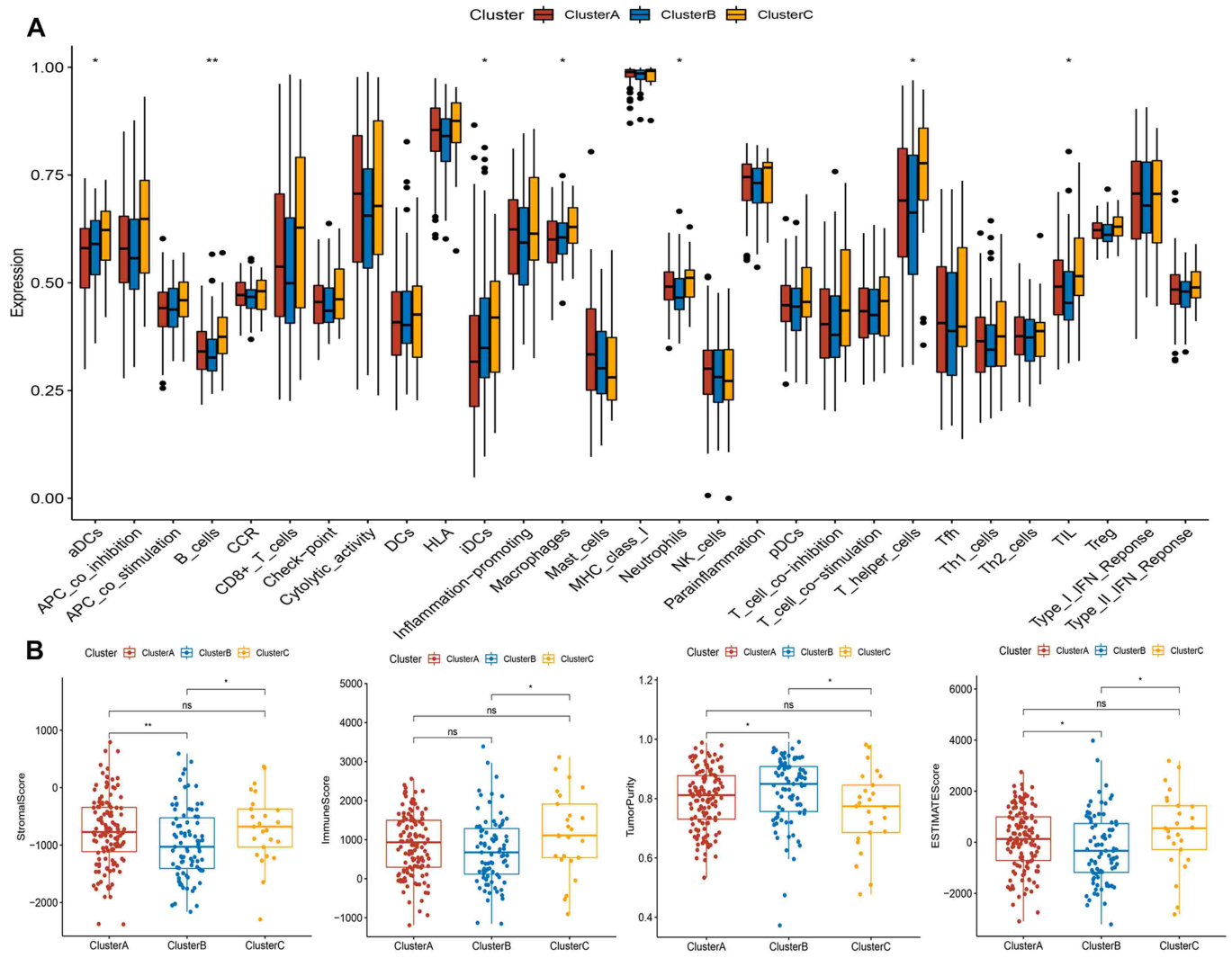

FIGURE 3. Immune cell infiltration. (A) ssGSEA analysis showed that different clusters displayed distinct immune cell infiltration. (B) Comparisons among the three clusters *via* ESTIMATE method *$p < 0.05$, **$p < 0.01$ and ***$p < 0.001$. aDCs, activated dendritic cells; APC, antigen presenting cell; CCR, CC chemokine receptor; DCs, dendritic cells; iDCs, immature dendritic cells; MHC, major histocompatibility complex; NK, natural killer; pDCs, plasmacytoid dendritic cells; Tfh, T follicular helper; Th1, Type 1 T helper cell; TIL, tumor infiltrating lymphocytes; Treg, regulatory T cells; IFN, interferon.

based on age, FIGO stage, grade and risk score (Fig. 5A). The calibration plots illustrated good consistency between the observed overall survival rate and the predicted survival rates at 1, 3 and 5 years (Fig. 5B). To assess the clinical practicality of our NRGscore signature, we performed decision curve analysis, which takes into account the preferences of patients and clinicians and involves weighing the benefits and harms associated with the prediction model. Comparison of the performance of variables such as age, FIGO stage, grade, risk score and the nomogram indicated that the nomogram demonstrated the best predictive ability (Fig. 5C).

3.9 Stratification analyses of the NRGscore model in immune features

We evaluated the infiltration levels of immune cells and immune checkpoint molecules to investigate the association between our NRGscore model, the tumor immune microenvironment and immunotherapeutic response. Using the CIBERSORT deconvolution algorithm, we found that the low-risk group exhibited elevated levels of immune cell infiltration, including $CD8^+$ T cells, regulatory T cells (Tregs), resting NK cells, and resting dendritic cells. Conversely, the levels of macrophages M0, activated dendritic cells, activated mast cells and neutrophils were significantly decreased in the low-risk group (Fig. 6A). We further validated the distinct proportions of immune cell infiltration and functions using the ssGSEA algorithm. The low-risk group showed significantly increased proportions of B cells, macrophages, $CD8^+$ T cells, NK cells, neutrophils, T helper cells and tumor-infiltrating lymphocytes (TILs). Additionally, the activity of immune functions, particularly inflammation promotion, checkpoint regulation, and human leukocyte antigen (HLA) expression, was significantly elevated in patients with low risk scores ($p < 0.001$) (**Supplementary Fig. 6A**). Moreover, we used the ESTIMATION algorithm to predict the content of stromal cells and immune cells and then calculated the ESTIMATE score by combining them. The low-risk group exhibited higher estimate scores, stromal scores, and immune scores (Fig. 6B).

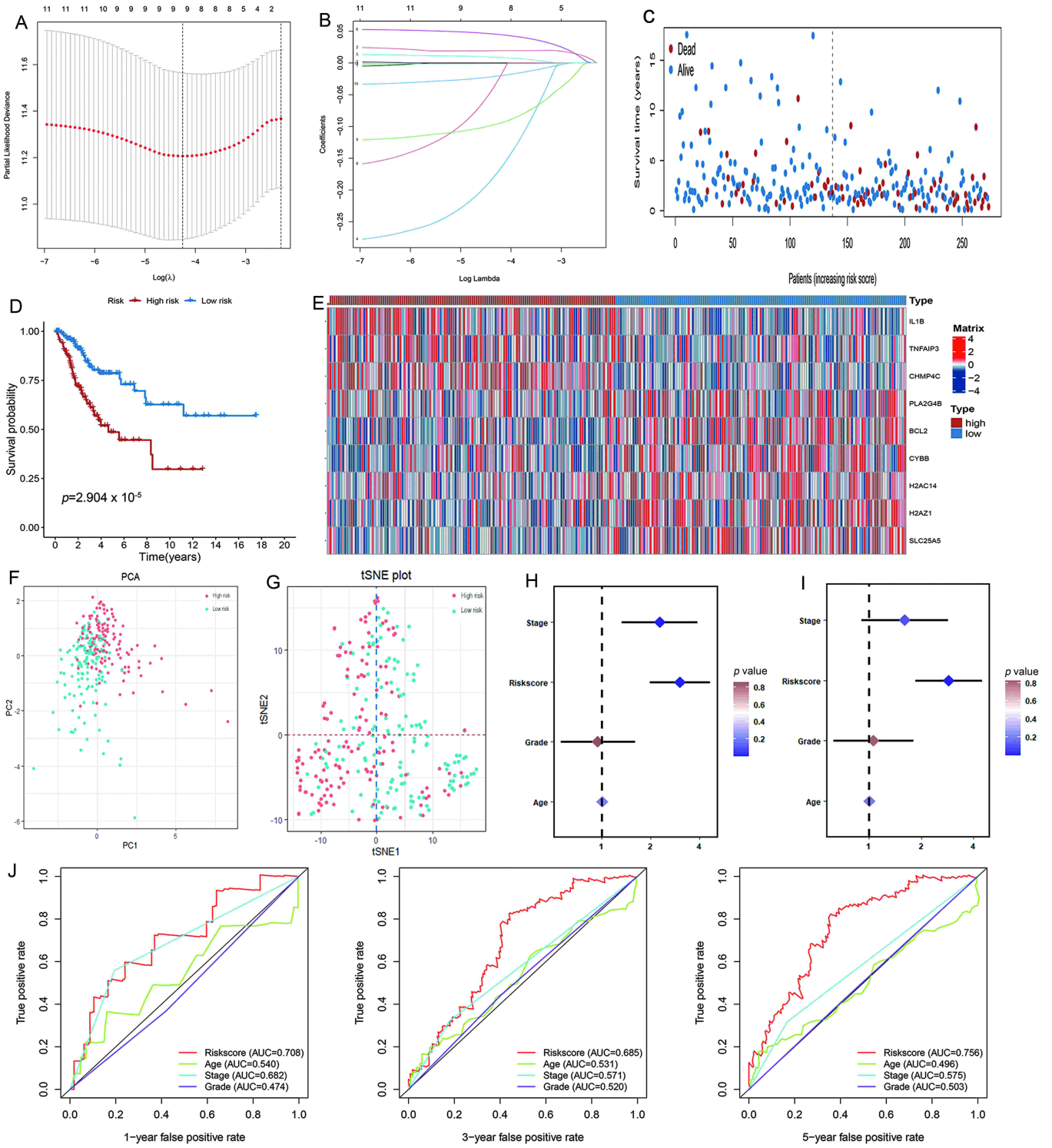

FIGURE 4. Construction and evaluation of necroptosis-related gene signature. (A) The value of the super parameter λ in the LASSO regression model was determined using 10-fold cross-validation. (B) The overview of LASSO coefficients. (C) Distribution of survival status and risk score in CC patients. (D) Survival analysis for the low- and high-risk groups. (E) The heatmap demonstrated the differences with regard to the necroptosis-related genes between comparison groups. (F) Principal component analysis (PCA) for the expression of necroptosis-related regulators to distinguish patients in high-risk group from those in low-risk group. (G) T-distributed stochastic neighbor embedding (tSNE) was utilized for dimension reduction and to visualize the diversity of the patients between high- and low-risk groups. (H) Univariate regression analysis demonstrated that the risk score and FIGO stage remarkably correlated with prognosis. (I) Multivariate analysis indicated that risk score could independently predict the prognosis. (J) The ROC curves and area under the curves (AUC) compared the necroptosis-related gene signature with other clinical and pathological factors.

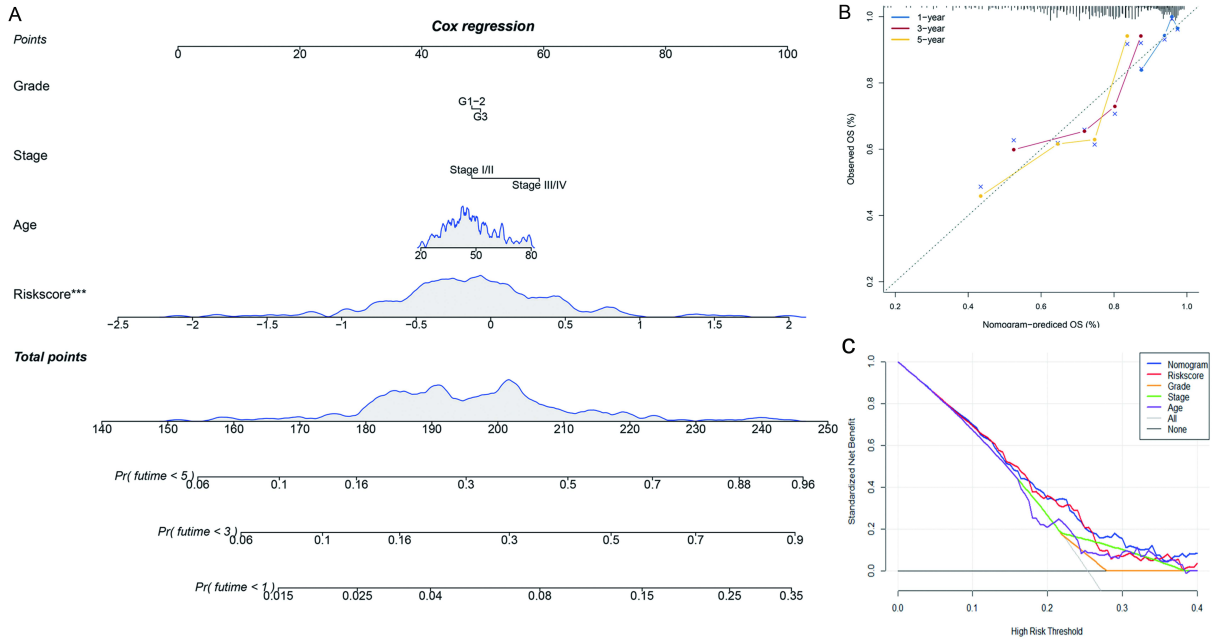

FIGURE 5. Nomogram construction and evaluation of prognostic ability of NRGscore signature. (A) Nomogram construction to predict the probability of patient mortality *via* four characteristics. (B) Calibration curve. (C) Decision curve analysis (DCA).

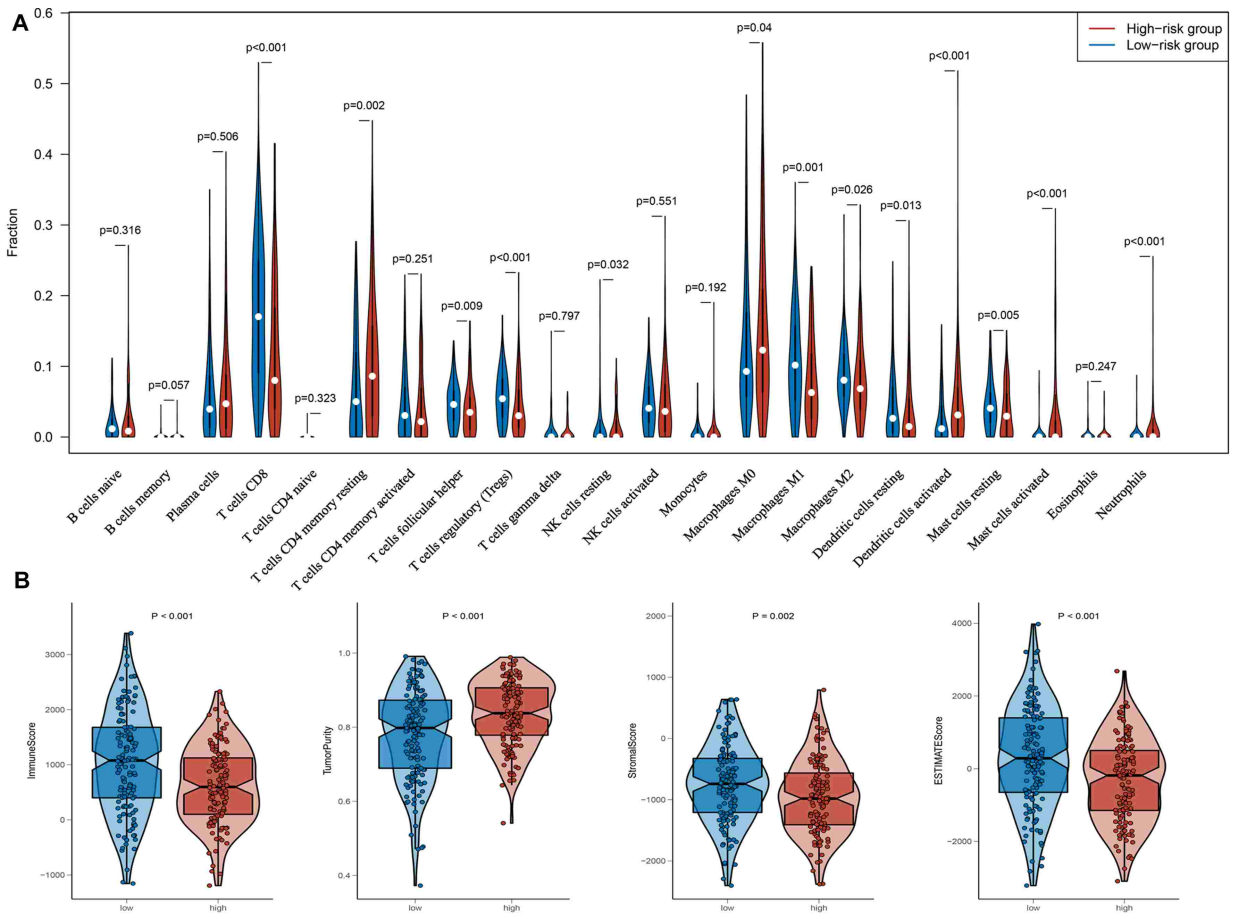

FIGURE 6. TME immune cell infiltration in high- and low-risk groups. (A) CIBERSORT deconvolution algorithm revealed the infiltrating levels of 22 immune cell types in comparison groups. (B) Immune score, tumor purity, stromal score, and estimate score in comparison groups are shown.

Spearman correlation analysis revealed an inverse relationship between the risk score and most immune cell populations (**Supplementary Fig. 6B**). Furthermore, we explored the relationship between the infiltration levels of immune cells and the prognosis of CC patients. The results demonstrated that patients with higher infiltration levels of Tregs ($p = 0.003$), resting mast cells ($p = 0.009$), and $CD8^+$ T cells ($p = 0.03$) exhibited better prognoses compared to those with lower infiltration levels (**Supplementary Fig. 6C–E**).

3.10 Comparison of mutation status between high- and low-risk groups

To explore the mechanisms underlying the predictive ability of the NRGscore signature for CC patient prognosis, we analyzed the status of single nucleotide polymorphisms (SNPs) in our model. The top 20 genes with the highest mutation rates are displayed in Fig. 7A,B. In the high-risk group, the five genes with the highest alteration frequencies were phosphatidylinositol-4,5-bisphosphate 3-kinase catalytic subunit alpha (*PIK3CA*) (25%), titin (*TTN*) (24%), lysine methyltransferase 2c (*KMT2C*) (19%), mucin 16, cell surface associated (*MUC16*) (17%) and filaggrin (*FLG*) (14%), while those genes in the low-risk group were *TTN* (33%), *PIK3CA* (27%), *KMT2C* (19%), *DMD* (16%) and *MUC16* (16%). Then, we investigated the mutation status of 9 necroptosis-related genes in the cBioPortal database. The mutation frequencies, from high to low, were as follows: *TNFAIP3*, *SLC25A5*, *CYBB*, *CHMP4C*, *H2AZ1*, *H2AC14*, *PLA2G4B*, *BCL2* and *IL1B* (**Supplementary Fig. 7**). In our NRGscore signature, we did not find a significant correlation between the risk score and TMB (Fig. 7C). However, when patients were divided into four groups based on the combination of NRGscore and TMB levels, the results demonstrated that patients with high TMB levels and low risk scores had a better survival rate compared to those with low TMB levels and high risk scores ($p < 0.001$, Fig. 7D). These results suggest that patients with lower risk scores and higher TMB levels may exhibit better response and derive more benefit from immunotherapy.

3.11 Copy number variants (CNV) pattern of the necroptosis-related genes

Copy number variants refer to the structural variations of DNA that involve a gain or loss of a specific region of the genome, leading to changes in the copy number of genes. CNVs have been implicated in the pathogenesis of various diseases, including cancer, autoimmune disorders and neurodegenerative diseases. The copy number variants were obtained from UCSC dataset. Investigating the CNV landscape of differentially expressed necroptosis-related genes represented an important step in understanding the genetic basis of necroptosis-related diseases and may lead to new strategies for prevention, diagnosis and treatment. Actually, we found that almost all genes presented CNVs with regard to the loss or gain of DNA copies (**Supplementary Fig. 8**).

3.12 Evaluation of the CC patients' response to immunotherapy

To investigate the association of immune-oncology targets with the NRGscore signature, we compared the expression levels of immune checkpoint genes in this model. The results demonstrated that most of these immune checkpoint genes were significantly elevated in the low-risk group (Fig. 8A). Furthermore, we assessed the correlation between the risk score and immune checkpoints using Spearman analysis. The results showed a significant negative correlation between the risk score and the expression levels of programmed cell death 1 (PD-1) ($R = -0.34$; $p < 0.001$) and cytotoxic t-lymphocyte associated protein 4 (*CTLA-4*) ($R = -0.29$; $p < 0.001$) (Fig. 8E), indicating that patients with low risk score potentially had better response to PD-1 and CTLA-4 antibodies. Next, we investigated the correlation between the NRGscore signature and immunotherapeutic biomarkers using the TIDE database. The results demonstrated that the TIDE and Exclusion scores were significantly decreased, while the Dysfunction score was substantially increased in the low-risk group (Fig. 8C). This suggests that patients with a lower risk score may respond better to immune checkpoint blockade, while those with a higher risk score may exhibit a greater propensity for tumor immune escape and resistance to cancer immunotherapies. Furthermore, we calculated the antitumor immune cytolytic activity score (CYT) using the geometric mean of the expression levels of the genes perforin 1 (*PRF1*) and granzyme A (*GZMA*). The gene expression profiles of *GZMA*, *PRF1* and CYT score were negatively correlated with the risk score, indicating that higher expression of *GZMA* and *PRF1* was associated with improved prognosis, consistent with prior studies (Fig. 8B,D) [16, 17]. Additionally, we also conducted IPS analyses and found that patients with low risk scores demonstrated higher levels of IPS though the difference was not significant (**Supplementary Fig. 9A**). Stemness indices, which measure the stemlike characteristics of tumor cells, have been associated with poor immunotherapy response in previous studies and can serve as an indicator for potential immune treatment outcomes. Analysis of the relationship between the risk score and mRNAsi showed no noticeable difference between them (**Supplementary Fig. 9B**). Furthermore, we investigated the correlation of the NRGscore signature with the response to immunotherapy using the IMvigor210 immunotherapy cohort. However, we did not find a significant difference between the high- and low-risk groups in terms of response to immunotherapy (**Supplementary Fig. 9C,D**).

3.13 Analysis of pathway and process enrichment

First, we obtained 159 necroptosis-related DEGs, based on which functional enrichment analyses were conducted. The biological processes associated with these DEGs were primarily related to programmed necrotic cell death and necroptotic processes. The cell composition analysis revealed associations with the endosomal sorting complex required for transport (ESCRT) III complex, nucleosomes and DNA packaging complexes. In terms of molecular function, the DEGs were primarily involved in cytokine receptor binding (Fig. 9A). We

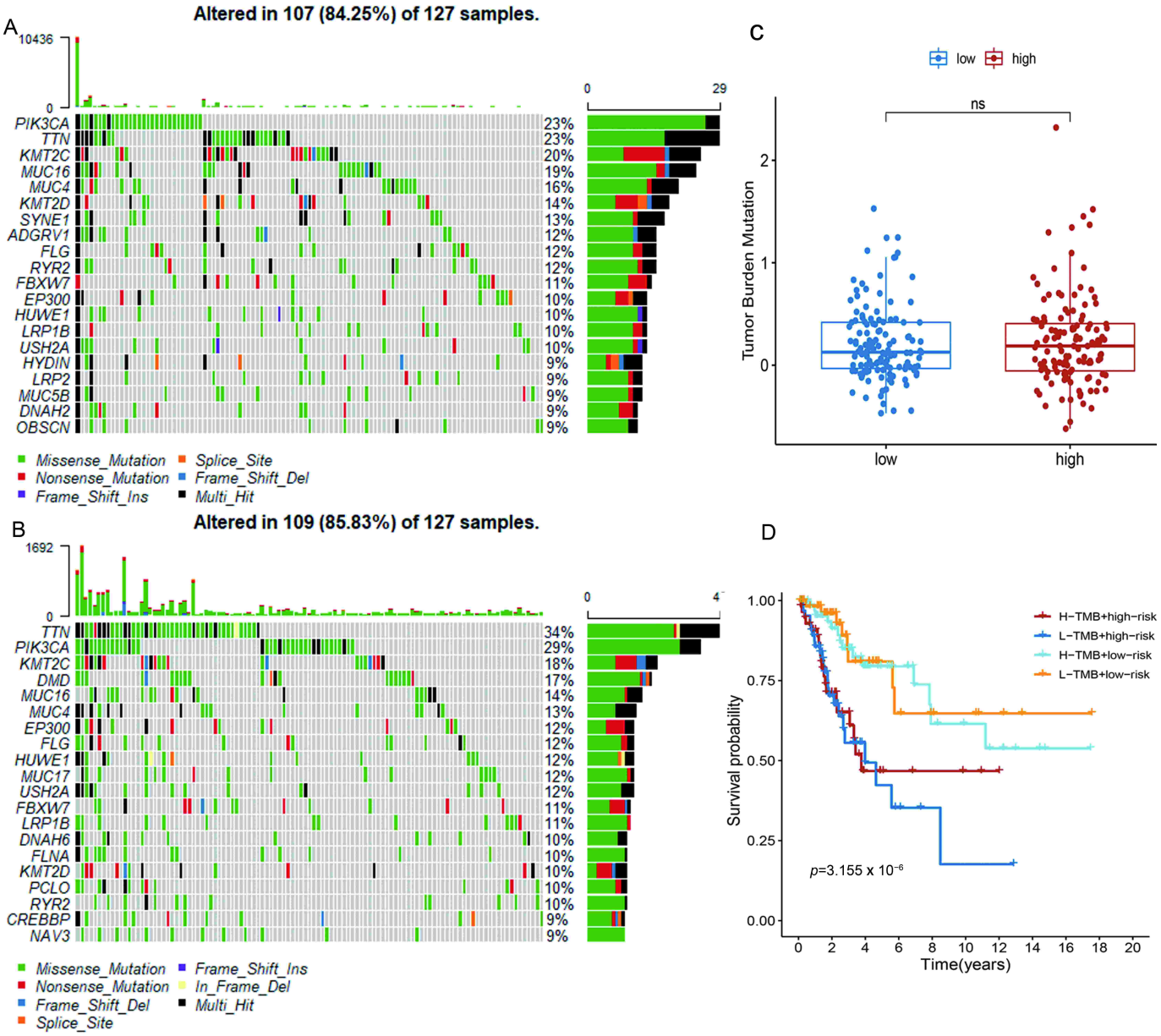

FIGURE 7. Tumor somatic mutation landscape. Distribution of the top 20 variant mutated genes between high- (A) and low-risk (B) groups. (C) Differences in tumor mutation burden (TMB) among different risk groups. (D) Survival analyses of patients with different TMB combined with risk score are presented. DMD, dystrophin; MUC4, mucin 4, cell surface associated; EP300, e1a binding protein p300; huwe1, hect, uba and wwe domain containing e3 ubiquitin protein ligase 1; MUC17, mucin 17, cell surface associated; USH2A, usherin; FBXW7, f-box and wd repeat domain containing 7; LRP1B, ldl receptor related protein 1b; DNAH6, dynein axonemal heavy chain 6; FLNA, filamin A; KMT2D, lysine methyltransferase 2d; PCLO, piccolo presynaptic cytomatrix protein; RYR2, ryanodine receptor 2; CREBBP, creb binding protein; NAV3, neuron navigator 3.

further conducted KEGG pathway analysis, which revealed that the DEGs were significantly enriched in pathways such as necroptosis, apoptosis, tumor necrosis factor (TNF) signaling, nuclear factor kappa light chain enhancer of activated B cells (NF-κB) signaling pathways, *etc.*, indicating that these NRGs may be involved in tumorigenesis, tumor progression and antitumor immunity of cervical cancer (Fig. 9B). Additionally, GSEA was performed to investigate the pathway enrichment patterns associated with the risk scores. Patients with high risk scores showed enrichment in tumor-related pathways, including apoptosis, nucleotide-binding and oligomerization domain (NOD)-like receptor signaling, and MAPK signaling pathways (Fig. 9C). On the other hand, patients with low risk scores exhibited enhanced enrichment in immune-related pathways, such as systemic lupus erythematosus and janus kinase - signal transducers and activators of transcription (JAK-STAT) signaling pathway (Fig. 9D). These results indicate that the differences in prognosis and immunogenicity between high- and low-risk patients may be attributed to distinct features in the TME.

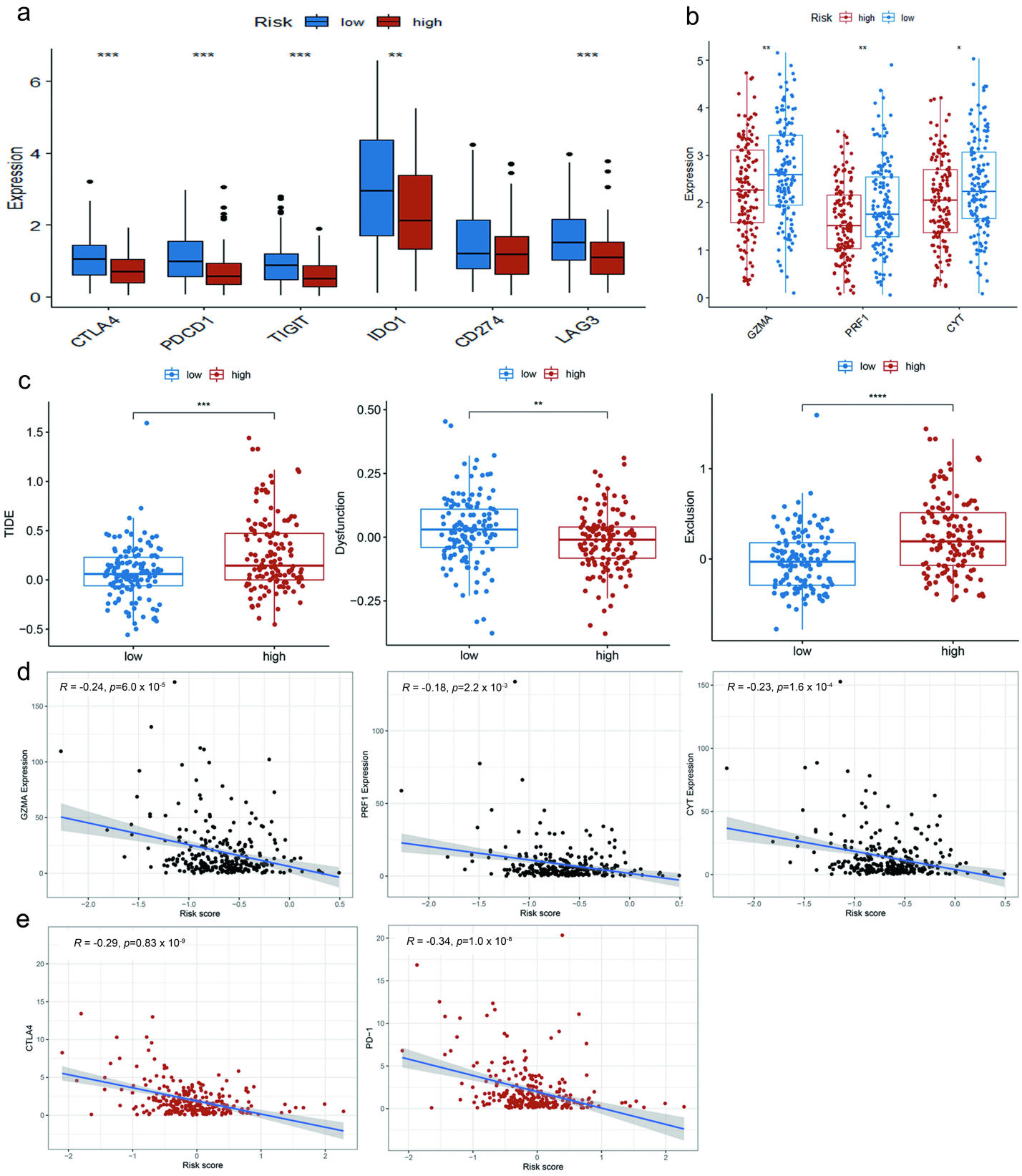

FIGURE 8. Assessment of the patient's response to the immunotherapy. (A) Comparison of the expression levels of immune checkpoint genes in high-risk patients versus those at low risk for the disease. (B) The variances in GZMA, PRF1 and CYT expression between comparison groups. (C) Prediction of the sensitivity to immunotherapy through Tumor Immune Dysfunction and Exclusion database. (D) Spearman analyses were conducted to assess the association between the risk score and GZMA, PRF1 and CYT score. (E) Correlation between risk score and immune checkpoint genes. TIGIT, T cell immunoreceptor with Ig and ITIM domains; IDO1, indoleamine 2,3-Dioxygenase 1; CD274, CD274 Molecule; LAG3, lymphocyte Activating 3.

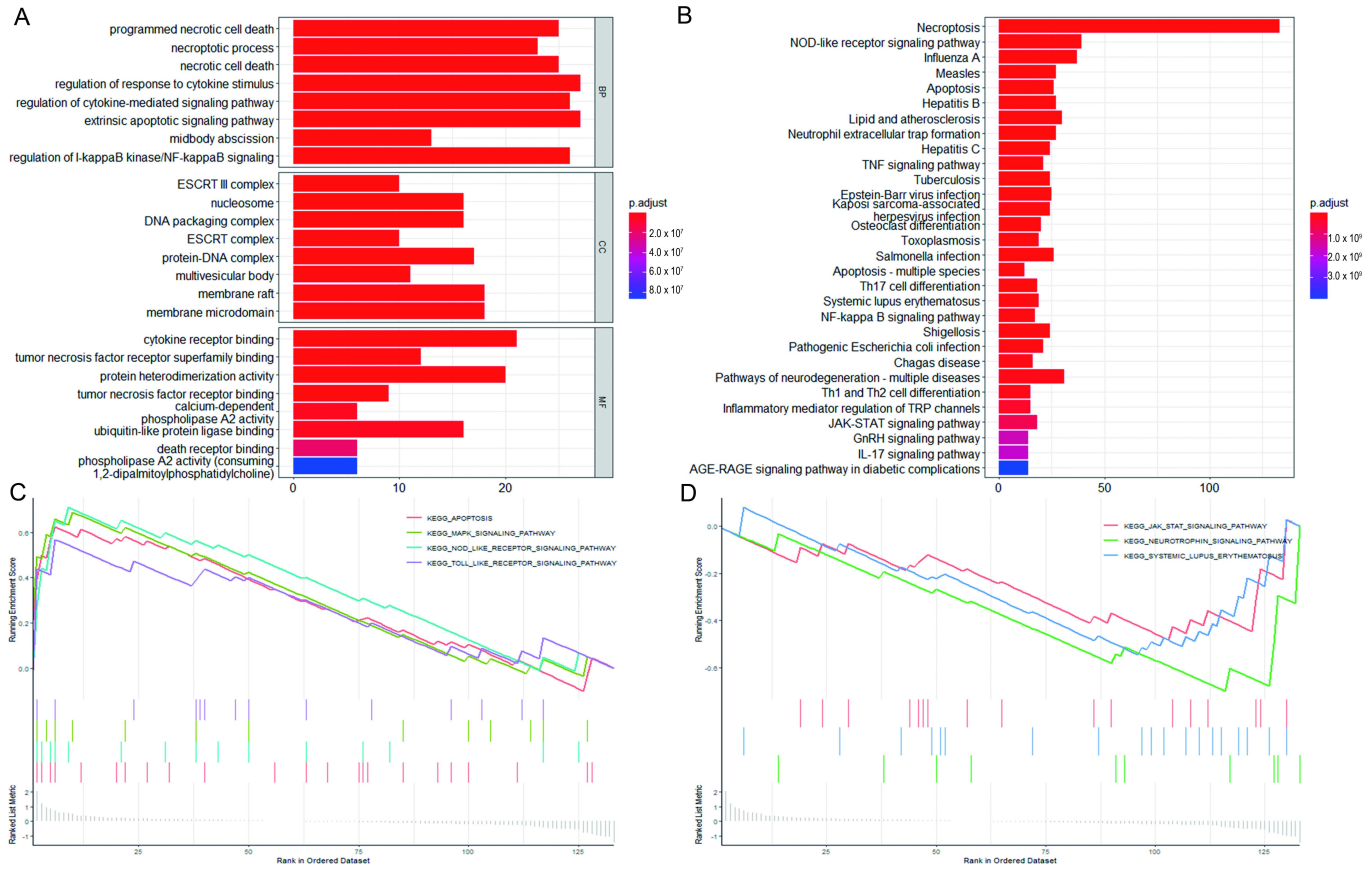

FIGURE 9. Functional enrichment analysis. (A) GO analysis. (B) KEGG pathways analysis. (C,D) GSEA analysis in (C) high-risk cohort and (D) low-risk cohort. GnRH, gonadotropin-releasing hormone; IL-17, interleukin-17; AGE-RAGE, advanced glycation end products (ages), receptor for ages; MAPK, mitogen-activated protein kinase.

3.14 Identification of potential anti-cancer drugs and compounds

To identify potential chemotherapy targets for treating patients with CC based on the NRGscore signature, we evaluated the IC50 (half maximal inhibitory concentration) of seven drugs between the high- and low-risk groups. We found that the IC50 values of cisplatin, temsirolimus, etoposide and gemcitabine were decreased in patients with low risk scores, indicating potential sensitivity to these drugs, while the IC50 value of docetaxel was elevated in patients with high risk scores (Fig. 10A). Next, we searched for 300 DEGs in the CMap database to evaluate the mechanism of action (MoA) and targeted compounds. We identified 22 MoAs that were correlated with 28 compounds. Among these compounds, four (cycloheximide, cephaeline, verrucarin-A and emetine) shared the MoA of protein synthesis inhibitor, while ingenol, phorbol-12-myristate-13-acetate and prostratin shared the MoA of the protein kinase c (PKC) activator (Fig. 10B).

3.15 Validation of the key NRGs by qRT-PCR in CC clinical samples

We evaluated the mRNA expression levels of nine key NRGs in CC patients' tissues using qRT-PCR. The results revealed that *BCL2*, *SLC25A5* and *H2AZ1* were significantly upregulated in cancer tissues (Fig. 11A), while *TNFAIP3* and *H2AC14* were markedly upregulated in adjacent noncancerous samples, which were consistent with the results obtained from the bioinformatic analyses.

To further investigate the protein expression of these five differentially expressed genes (*BCL2*, *SLC25A5*, *H2AZ1*, *TNFAIP3* and *H2AC14*), we searched for representative images of immunohistochemistry staining from the HPA database. The images demonstrated that these hub genes were remarkably overexpressed in CC samples compared to normal tissues (Fig. 11B).

4. Discussion

CC is one of the most frequently occurring gynecologic malignancies worldwide. Despite notable advancements in therapy, the 5-year survival rate for patients with recurrent cervical cancer remains alarmingly low, at less than 5%. Therefore, it is crucial to discover specific biomarkers and develop risk-stratification algorithms to improve prognosis prediction and guide treatment decisions for CC patients.

In recent years, there has been considerable research on the relationship between abnormal expression of NRGs and the development of tumors. Key regulators of necroptosis, such as *RIPK3*, *MLKL* and cylindromatosis (*CYLD*), have been found to be suppressed in various tumor cell lines and types. Additionally, necroptotic cell death has been shown to induce and enhance antitumor immune responses in the TME [18]. However, some studies have suggested that necroptosis can

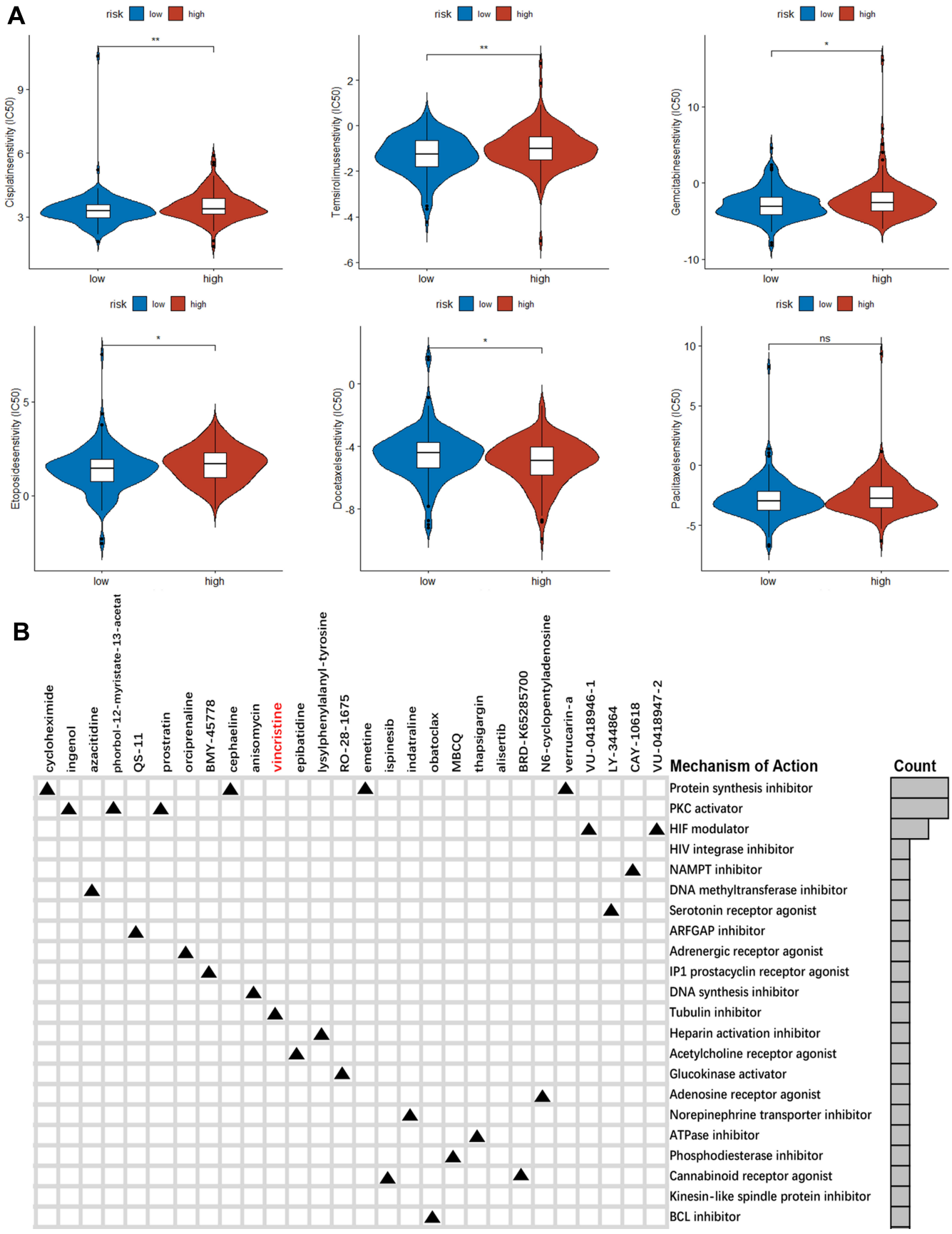

FIGURE 10. Identification of potential anti-cancer drugs and compounds. (A) Chemotherapy drug sensitivity result. (B) CMap database results to investigate the mechanism of action (MoA) and targeted compounds. PKC, protein kinase C; HIF, hypoxia-inducible factor; NAMPT, nicotinamide phosphoribosyltransferase; ARFGAP, ADP Ribosylation Factor GTPase Activating Protein; BCL, B-cell leukemia/lymphoma.

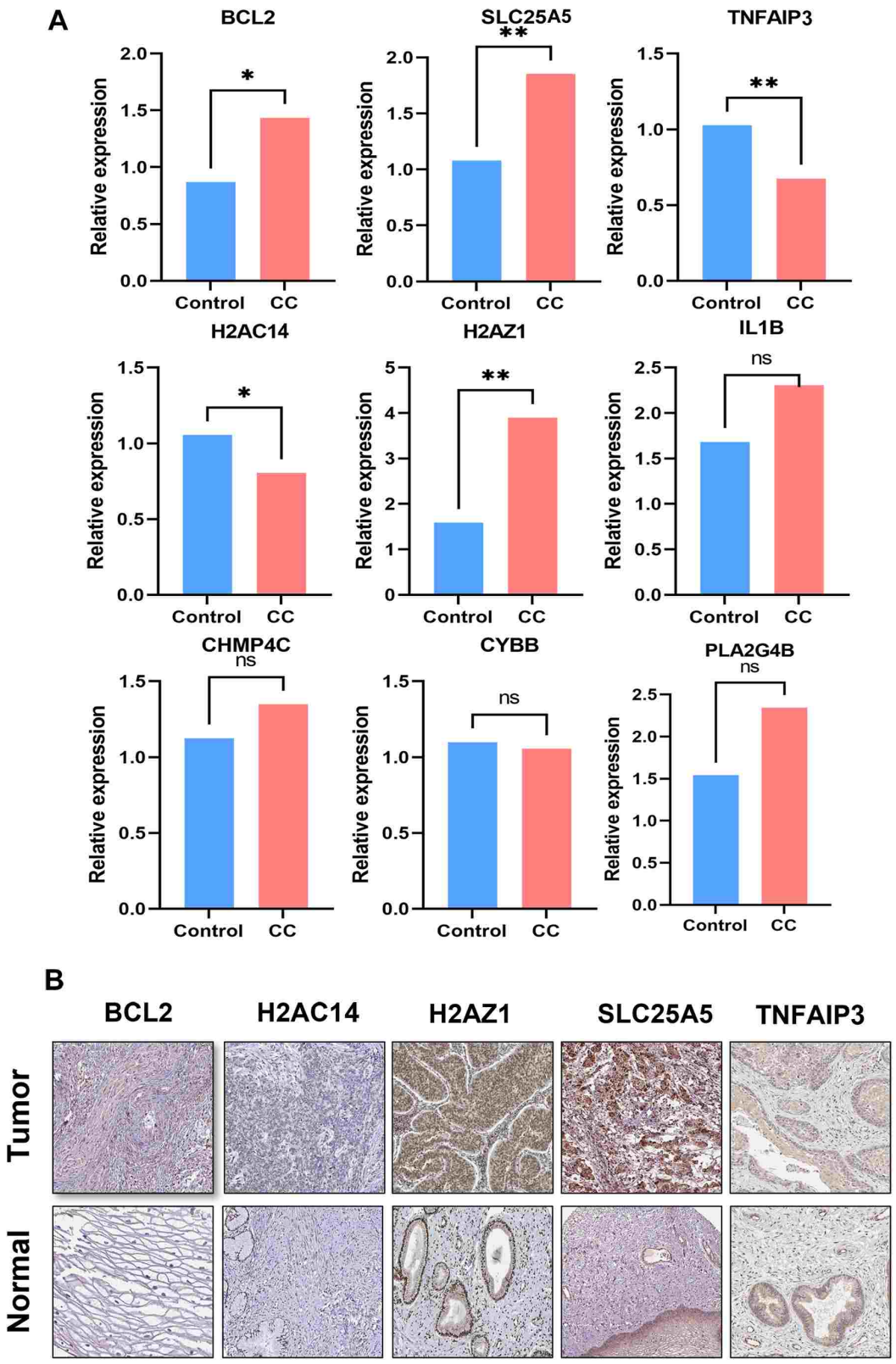

FIGURE 11. Validation of the nine NRGs by qRT-PCR and immunohistochemistry analysis. (A) The mRNA expression of H2AZ1, H2AC14, PLA2G4B, BCL2, CYBB, SLC25A5, IL1B, TNFAIP3 and CHMP4C in clinical samples. (B) Immunohistochemistry of five hub genes from the HPA database. *$p < 0.05$, **$p < 0.01$. IL1B, interleukin-1B; H2AZ1, H2A.Z variant histone 1; H2AC14, H2A clustered histone 14; TNFAIP3, TNF alpha induced protein 3; CHMP4C, charged multivesicular body protein 4c; PLA2G4B, phospholipase a2 group ivb; BCL2, BCL2 apoptosis regulator; CYBB, cytochrome b-245 beta chain; SLC25A5, solute carrier family 25 member 5.

also promote tumor progression [19, 20]. Overall, necroptosis is involved in tumorigenesis, tumor progression and antitumor immunity in several cancer types. Since NRGs hold potential as prognostic and predictive biomarkers for CC patients, we focused on 51 differentially expressed NGRs in 303 tumor tissues and 10 normal samples. Through univariate Cox regression analysis, eleven prognostic NRGs were identified. Utilizing unsupervised consensus clustering analysis based on the expression patterns of these NRGs, we classified patients into three distinct clusters, which exhibited variations in clinical characteristics, prognosis, TME immune cell infiltration and sensitivity to chemotherapy. Furthermore, by employing LASSO regression analysis, we selected nine key NRGs (*H2AZ1*, *H2AC14*, *PLA2G4B*, *BCL2*, *CYBB*, *SLC25A5*, *IL1B*, *TNFAIP3* and *CHMP4C*) to construct a prognostic risk score model.

Most NRGs presented in our signature correlated with CC tumorigenesis and proliferation. *CYBB*, also named as NOX2, is a critical component of the membrane-bound oxidase of phagocytes that generates superoxide, and its expression mediates the interferon-based immune defense against HPV infection and is associated with favorable prognosis in CC patients [21]. The therapeutic approaches to treat cervical cancer, including radiation, chemotherapy and immune-based therapy, usually produced a marked effect through the induction of apoptosis, which can be triggered by intrinsic and extrinsic pathways. In addition, this intrinsic pathway can be triggered by members of the *BCL2* family of proteins and downstream mitochondrial signals [22–24]. In a study by Xie *et al.* [25], punicalagin was shown to promote autophagic degradation of HPV and downregulate the levels of the major HPV oncoproteins E6 and E7 in cervical cancer cells by activating the reactive oxidative species - c-Jun N-terminal kinase (ROS-JNK) pathway and promoting the phosphorylation of *BCL2*. *SLC25A5* overexpression has been identified as an independent prognostic factor in colon cancer patients, where it represses cell growth by inhibiting the MAPK signaling pathway [26]. IL1B has also been found to be an independent prognostic factor, and its high levels have been associated with delayed disease progression in triple-negative breast carcinoma [27]. *H2AZ1*, as one isoform of *H2AZ*, plays a pivotal role in hepatocarcinogenesis by modulating the cell cycle and epithelial-mesenchymal transition (EMT)-regulatory proteins [28]. *TNFAIP3* expression levels are regulated by miR-214 in cervical cancer cells, and its effects can vary depending on the cell types involved [29]. For instance, Lee *et al.* [30] reported that *TNFAIP3* overexpression in triple-negative breast cancer cells could induce an aggressive phenotype, while in other breast cancer cells, it may induce apoptosis, further confirming that the effects of *TNFAIP3* may vary depending on the cell types. *CHMP4C*, which modulates EMT, has been shown to contribute to the survival and mobility of cervical cancer cells. Overexpression of *CHMP4C* in cervical cancer tissues is associated with poor overall survival [31].

Recent research has indicated that the activation of the NF-κB signaling pathway promotes the growth of cervical cancer and increases the production of tumor necrosis factor-alpha (TNF-α) [32]. The TNF signaling pathway is involved in balancing cell survival and necroptosis, a form of programmed cell death [33]. Additionally, the differentiation of Th17 cells is regulated by miR-146a, which modulates cervical cancer cell growth and apoptosis through the NF-κB signaling pathway by targeting TRAF6 [34]. These findings suggest that necroptosis-related genes may be involved in the tumorigenesis and progression of cervical cancer through both tumor-related and immune-related pathways. However, further research is needed to fully understand the mechanisms by which these necroptosis-related genes contribute to CC. Further, patients with a low risk score in our study showed enrichment in systemic lupus erythematosus (SLE) and the JAK-STAT signaling pathway, indicating that the differences in prognosis and immunogenicity between high- and low-risk patients may be attributed to distinct features in the TME of these patient groups.

The proposed NRGscore signature demonstrated independent and reliable characteristics for predicting the prognosis of CC patients. This was evident from the results of various analyses, including Kaplan-Meier survival analyses, the AUC values of ROC curves for predicting 1-, 3- and 5-year survival rates, correlation analyses between clinical features and risk scores, and univariate and multivariate Cox regression analyses considering clinicopathological traits. The NRGscore signature showed a good discriminatory performance in terms of patient prognosis, regardless of age, grade, pathological type or FIGO stage. Furthermore, patients with high risk scores were more likely to exhibit clinicopathological characteristics and molecular subtypes associated with high malignancy, while patients with low risk scores showed the opposite trend.

In this study, we compared the degree of immune cell infiltration and immune function in relation to the NRGscore. We found that patients with a high risk score had a lower percentage of immune cell infiltration and weaker antitumor immune response. Dendritic cells are key components of the system for antigen processing and presentation [35]. The risk score showed a negative correlation with resting dendritic cells and a positive correlation with activated dendritic cells, indicating a potential dysfunction in the antigen processing and presentation system associated with a high risk score. NK cells, which play critical roles in tumor immune surveillance, demonstrated prognostic significance, with reduced NK cell function linked to worse prognosis in cancer patients [36, 37]. Neutrophils exhibited diverse roles in different tumors, promoting cancer growth and migration in some types (*e.g.*, pancreatic cancer, hepatocellular carcinoma, and breast cancer) [38–40] while inhibiting lymph node metastasis in others (*e.g.*, Epstein-Barr virus-associated gastric carcinoma) [41]. $CD8^+$ T cells, known for their tumor-suppressive function, have been associated with improved prognosis in various cancers [42]. The composition and numbers of TILs are considered important indicators of the host immune response to tumors and have shown good prognostic value [43]. Our study revealed that patients with a low risk score had significantly higher proportions of $CD8^+$ T cells and TILs, leading to a better prognosis than patients with a high risk score.

Immune checkpoint inhibitors (ICIs), such as CTLA-4 and PD-1 targeted therapies, have shown promising response rates in recurrent and metastatic tumors, including CC, with CTLA-4 and PD-1 being the most commonly targeted molecules.

These therapies have demonstrated durable responses and lower toxicity than traditional chemotherapeutic drugs [44, 45]. We found that patients with a low risk score, based on our NRGscore signature, had elevated expression levels of immune checkpoint molecules such as PD-1, CTLA-4 and T cell immunoreceptor with Ig and ITIM domains (TIGIT). This suggests that ICIs may be more effective in low-risk patients. Currently, Pembrolizumab, targeting the PD-1 receptor, is the only FDA-approved ICI for recurrent or metastatic CC [46]. There are many ongoing phase II and phase III clinical trials, such as NCT03830866 (CALLA), CT04221945 (KEYNOTE-A18) and NCT03635567 (Keynote-826), which will provide more novel evidence to evaluate the value of ICIs in CC patients. Several studies have demonstrated that the correct timing, combinations and sequencing of chemotherapy might promote antitumor immunity by affecting the TME. Additionally, combining ICIs with chemotherapy and radiation can induce cell death and antigen presentation and block immunosuppressive pathways, and holds promise for overcoming immunotherapy resistance in CC [47].

In this study, we observed that low-risk CC patients were more responsive to cisplatin, temsirolimus, etoposide and gemcitabine, while high-risk patients showed increased sensitivity to docetaxel. This information can guide the development of individualized treatment plans for CC patients based on their risk groups. We searched the CMap database for small molecular compounds to explore potential therapeutic options and identified 20 compounds, including vincristine, cycloheximide, phorbol-12-myristate-13-acetate and prostratin. Previous research has demonstrated that vincristine, in combination with cisplatin and intensity-modulated radiation therapy, showed optimized clinical efficacy and safety for advanced-stage CC patients [48]. Cycloheximide had been shown to reverse chemotherapy resistance in prostate cancer cells by inhibiting heat shock protein function [49]. Sung *et al.* [50] found that phorbol-12-myristate-13-acetate induces invasion and migration of HeLa cancer cells, which can be suppressed by the antioxidant 6-hydroxy-2,5,7,8-tetramethylchroman-2-carboxylic acid. Additionally, prostratin has been shown to exert anti-cancer effects by down-regulating the expression of chemokine receptor type 4 through the inhibition of salt-inducible kinase 3 (SIK3) expression in breast cancer cells [51].

This study has several limitations that should be acknowledged. Firstly, the NRGscore signature was constructed using data solely from public databases, and external validation with real-world data and larger sample sizes is necessary to confirm its reliability and generalizability. Future studies should aim to include diverse populations and additional clinical information to improve the robustness of the signature. Secondly, the use of ICIs in CC is still relatively new, and there is a lack of available immunotherapy data specific to this disease. Thus, further research and clinical trials are needed to generate more comprehensive and reliable evidence regarding the effectiveness of ICIs in CC treatment.

5. Conclusions

In conclusion, the proposed NRGscore signature could independently predict the prognosis of CC patients and is closely associated with the tumor microenvironment, chemotherapy response and immunotherapy outcomes, thereby contributing to our understanding of the mechanisms underlying CC carcinogenesis, tumor development and antitumor immunity. The identified necroptosis-related genes could be promising targets for improving immunotherapy outcomes and enabling individualized treatment approaches in CC patients.

AVAILABILITY OF DATA AND MATERIALS

The datasets used and analyzed during the current study are available from the corresponding author on reasonable request.

AUTHOR CONTRIBUTIONS

YMD and YHS—contributed to the conception and design; YCH and MMQ—contributed to the statistical analysis and drafting of the manuscript; YMD—contributed to the data collection; YHS—contributed to the editing. All authors have approved the final version for submission.

ETHICS APPROVAL AND CONSENT TO PARTICIPATE

The experimental protocol was established based on the ethical guidelines of the Helsinki Declaration and was approved by the Human Ethics Committee of the First Affiliated Hospital of Ningbo University (Ethics number: 2022061A-YJ01). Prior to sample collection, all patients provided informed consent and had not undergone any radiotherapy or chemotherapy treatments.

ACKNOWLEDGMENT

The authors would like to express appreciation to all the cervical cancer patients of the First Affiliated Hospital of Ningbo University for their contributions.

FUNDING

This work was supported by Medical and Health Science and Technology Project of Zhejiang Province (2022KY303), Science and Technology Programs of Ningbo (202003N4289), and the Medical and Health Science and Technology Program of Zhejiang Province (2021440659).

CONFLICT OF INTEREST

The authors declare no conflict of interest.

SUPPLEMENTARY MATERIAL

Supplementary material associated with this article can be found, in the online version, at https://oss.ejgo.net/

files/article/1867407982756544512/attachment/Supplementary%20material.docx.

REFERENCES

[1] Sung H, Ferlay J, Siegel RL, Laversanne M, Soerjomataram I, Jemal A, *et al*. Global Cancer Statistics 2020: GLOBOCAN estimates of incidence and mortality worldwide for 36 cancers in 185 countries. CA: A Cancer Journal for Clinicians. 2021; 71: 209–249.

[2] Thongkhao P, Janmunee N, Tangkananan A. Prognostic factors for post-recurrence survival among patients with locally advanced cervical cancer who underwent definitive concurrent chemoradiation. Reports of Practical Oncology and Radiotherapy. 2022; 27: 615–623.

[3] Nguyen ES, Risbud A, Birkenbeuel JL, Murphy LS, Goshtasbi K, Pang JC, *et al*. Prognostic factors and outcomes of *de novo* sinonasal squamous cell carcinoma: a systematic review and meta-analysis. Otolaryngology—Head and Neck Surgery. 2022; 166: 434–443.

[4] Kokka F, Bryant A, Olaitan A, Brockbank E, Powell M, Oram D. Hysterectomy with radiotherapy or chemotherapy or both for women with locally advanced cervical cancer. Cochrane Database of Systematic Reviews. 2022; 8: CD010260.

[5] Yan J, Wan P, Choksi S, Liu Z. Necroptosis and tumor progression. Trends in Cancer. 2022; 8: 21–27.

[6] Qiu Q, Li Y, Zhang Y, Hou Y, Hu J, Wang L, *et al*. A prognosis model for clear cell renal cell carcinoma based on four necroptosis-related genes. Frontiers in Medicine. 2022; 9: 942991.

[7] Ren H, Zheng J, Cheng Q, Yang X, Fu Q. Establishment of a necroptosis-related prognostic signature to reveal immune infiltration and predict drug sensitivity in hepatocellular carcinoma. Frontiers in Genetics. 2022; 13: 900713.

[8] Zhou X, Zhang B, Zheng G, Zhang Z, Wu J, Du K, *et al*. Novel necroptosis-related gene signature for predicting early diagnosis and prognosis and immunotherapy of gastric cancer. Cancers. 2022; 14: 3891.

[9] Liu T, Guo L, Liu G, Dai Z, Wang L, Lin B, *et al*. Identification of necroptosis-related signature and tumor microenvironment infiltration characteristics in lung adenocarcinoma. Lung Cancer. 2022; 172: 75–85.

[10] Wang Z, Chen G, Dai F, Liu S, Hu W, Cheng Y. Identification and verification of necroptosis-related gene signature with prognosis and tumor immune microenvironment in ovarian cancer. Frontiers in Immunology. 2022; 13: 894718.

[11] Green DR. The coming decade of cell death research: five riddles. Cell. 2019; 177: 1094–1107.

[12] Bertheloot D, Latz E, Franklin BS. Necroptosis, pyroptosis and apoptosis: an intricate game of cell death. Cellular & Molecular Immunology. 2021; 18: 1106–1121.

[13] Tang R, Xu J, Zhang B, Liu J, Liang C, Hua J, *et al*. Ferroptosis, necroptosis, and pyroptosis in anticancer immunity. Journal of Hematology & Oncology. 2020; 13: 110.

[14] Tong X, Tang R, Xiao M, Xu J, Wang W, Zhang B, *et al*. Targeting cell death pathways for cancer therapy: recent developments in necroptosis, pyroptosis, ferroptosis, and cuproptosis research. Journal of Hematology & Oncology. 2022; 15: 174.

[15] Zhang T, Wang Y, Inuzuka H, Wei W. Necroptosis pathways in tumorigenesis. Seminars in Cancer Biology. 2022; 86: 32–40.

[16] Narayanan S, Kawaguchi T, Yan L, Peng X, Qi Q, Takabe K. Cytolytic activity score to assess anticancer immunity in colorectal cancer. Annals of Surgical Oncology. 2018; 25: 2323–2331.

[17] Rooney M, Shukla S, Wu C, Getz G, Hacohen N. Molecular and genetic properties of tumors associated with local immune cytolytic activity. Cell. 2015; 160: 48–61.

[18] Kroemer G, Galluzzi L, Kepp O, Zitvogel L. Immunogenic cell death in cancer therapy. Annual Review of Immunology. 2013; 31: 51–72.

[19] Seifert L, Werba G, Tiwari S, Giao Ly NN, Alothman S, Alqunaibit D, *et al*. The necrosome promotes pancreatic oncogenesis *via* CXCL1 and Mincle-induced immune suppression. Nature. 2016; 532: 245–249.

[20] Borst J, Ahrends T, Bąbała N, Melief CJM, Kastenmüller W. $CD4^+$ T cell help in cancer immunology and immunotherapy. Nature Reviews Immunology. 2018; 18: 635–647.

[21] Cho SY, Kim S, Son M, Kim G, Singh P, Kim HN, *et al*. Dual oxidase 1 and NADPH oxidase 2 exert favorable effects in cervical cancer patients by activating immune response. BMC Cancer. 2019; 19: 1078.

[22] Fulda S, Debatin K. Extrinsic versus intrinsic apoptosis pathways in anticancer chemotherapy. Oncogene. 2006; 25: 4798–4811.

[23] Kaufmann SH, Earnshaw WC. Induction of apoptosis by cancer chemotherapy. Experimental Cell Research. 2000; 256: 42–49.

[24] Ghobrial IM, Witzig TE, Adjei AA. Targeting apoptosis pathways in cancer therapy. CA: A Cancer Journal for Clinicians. 2005; 55: 178–194.

[25] Xie X, Hu L, Liu L, Wang J, Liu Y, Ma L, *et al*. Punicalagin promotes autophagic degradation of human papillomavirus E6 and E7 proteins in cervical cancer through the ROS-JNK-BCL2 pathway. Translational Oncology. 2022; 19: 101388.

[26] Chen Y-J, Hong W-F, Liu M-L, Guo X, Yu YY, Cui YH, *et al*. An integrated bioinformatic investigation of mitochondrial solute carrier family 25 (SLC25) in colon cancer followed by preliminary validation of member 5 (SLC25A5) in tumorigenesis. Cell Death & Disease. 2022; 13: 237.

[27] Pe KCS, Saetung R, Yodsurang V, Chaotham C, Suppipat K, Chanvorachote P, *et al*. Triple-negative breast cancer influences a mixed M1/M2 macrophage phenotype associated with tumor aggressiveness. PLOS ONE. 2022; 17: e0273044.

[28] Yang HD, Kim P, Eun JW, Shen Q, Kim HS, Shin WC, *et al*. Oncogenic potential of histone-variant H2a.Z.1 and its regulatory role in cell cycle and epithelial-mesenchymal transition in liver cancer. Oncotarget. 2016; 7: 11412–11423.

[29] Sen P, Ghosal S, Hazra R, Arega S, Mohanty R, Kulkarni KK, *et al*. Transcriptomic analyses of gene expression by CRISPR knockout of miR-214 in cervical cancer cells. Genomics. 2020; 112: 1490–1499.

[30] Lee E, Ouzounova M, Piranlioglu R, Ma MT, Guzel M, Marasco D, *et al*. The pleiotropic effects of TNFα in breast cancer subtypes is regulated by TNFAIP3/A20. Oncogene. 2019; 38: 469–482.

[31] Lin S, Wang M, Cao Q, Li Q. Chromatin modified protein 4C (CHMP4C) facilitates the malignant development of cervical cancer cells. FEBS Open Bio. 2020; 10: 1295–1303.

[32] Zeng R, Xiong X. Effect of NMB-regulated ERK1/2 and p65 signaling pathway on proliferation and apoptosis of cervical cancer. Pathology. Research and Practice. 2022; 238: 154104.

[33] Chaouhan HS, Vinod C, Mahapatra N, Yu SH, Wang IK, Chen KB, *et al*. Necroptosis: a pathogenic negotiator in human diseases. International Journal of Molecular Sciences. 2022; 23: 12714.

[34] Li T, Li M, Xu C, Xu X, Ding J, Cheng L, *et al*. miR-146a regulates the function of Th17 cell differentiation to modulate cervical cancer cell growth and apoptosis through NF-κB signaling by targeting TRAF6. Oncology Reports. 2019; 41: 2897–2908.

[35] Burgdorf S, Porubsky S, Marx A, Popovic ZV. Cancer acidity and hypertonicity contribute to dysfunction of tumor-associated dendritic cells: potential impact on antigen cross-presentation machinery. Cancers. 2020; 12: 2403.

[36] Shimasaki N, Jain A, Campana D. NK cells for cancer immunotherapy. Nature Reviews Drug Discovery. 2020; 19: 200–218.

[37] Albertsson PA, Basse PH, Hokland M, Goldfarb RH, Nagelkerke JF, Nannmark U, *et al*. NK cells and the tumour microenvironment: implications for NK-cell function and anti-tumour activity. Trends in Immunology. 2003; 24: 603–609.

[38] Purohit A, Saxena S, Varney M, Prajapati DR, Kozel JA, Lazenby A, *et al*. Host Cxcr2-dependent regulation of pancreatic cancer growth, angiogenesis, and metastasis. The American Journal of Pathology. 2021; 191: 759–771.

[39] Zhou S, Zhou Z, Hu Z, Huang X, Wang Z, Chen E, *et al*. Tumor-associated neutrophils recruit macrophages and t-regulatory cells to promote progression of hepatocellular carcinoma and resistance to Sorafenib. Gastroenterology. 2016; 150: 1646–1658.e17.

[40] Coffelt SB, Kersten K, Doornebal CW, Weiden J, Vrijland K, Hau C, *et al*. IL-17-producing $\gamma\delta$ T cells and neutrophils conspire to promote breast cancer metastasis. Nature. 2015; 522: 345–348.

[41] Abe H, Morikawa T, Saito R, Yamashita H, Seto Y, Fukayama M. In Epstein—Barr virus-associated gastric carcinoma a high density of CD66b-positive tumor-associated neutrophils is associated with intestinal-type histology and low frequency of lymph node metastasis. Virchows Archiv. 2016; 468: 539–548.

[42] St. Paul M, Ohashi PS. The roles of CD8$^+$ T cell subsets in antitumor immunity. Trends in Cell Biology. 2020; 30: 695–704.
[43] Tang Y, Zhang AXJ, Chen G, Wu Y, Gu W. Prognostic and therapeutic TILs of cervical cancer—current advances and future perspectives. Molecular Therapy—Oncolytics. 2021; 22: 410–430.
[44] Kooshkaki O, Derakhshani A, Safarpour H, Najafi S, Vahedi P, Brunetti O, *et al*. The latest findings of PD-1/PD-L1 inhibitor application in gynecologic cancers. International Journal of Molecular Sciences. 2020; 21: 5034.
[45] Ai L, Xu A, Xu J. Roles of PD-1/PD-L1 pathway: signaling, cancer, and beyond. Advances in Experimental Medicine and Biology. 2020; 8: 33–59.
[46] Mauricio D, Zeybek B, Tymon-Rosario J, Harold J, Santin AD. Immunotherapy in cervical cancer. Current Oncology Reports. 2021; 23: 61.
[47] Pitt J, Vétizou M, Daillère R, Roberti M, Yamazaki T, Routy B, *et al*. Resistance mechanisms to immune-checkpoint blockade in cancer: tumor-intrinsic and -extrinsic factors. Immunity. 2016; 44: 1255–1269.
[48] Zhang H, Zhang Y. Application of vincristine and cisplatin combined with intensity-modulated radiation therapy in the treatment of patients with advanced cervical cancer. American Journal of Translational Research. 2021; 13: 13894–13901.
[49] Gibbons NB, Watson RWG, Coffey RNT, Brady HP, Fitzpatrick JM. Heat-shock proteins inhibit induction of prostate cancer cell apoptosis. The Prostate. 2000; 45: 58–65.
[50] Sung HJ, Kim Y, Kang H, Sull JW, Kim YS, Jang SW, *et al*. Inhibitory effect of Trolox on the migration and invasion of human lung and cervical cancer cells. International Journal of Molecular Medicine. 2012; 29: 245–251.
[51] Alotaibi D, Amara S, Johnson TL, Tiriveedhi V. Potential anticancer effect of prostratin through SIK3 inhibition. Oncology Letters. 2018; 15: 3252–3258.

How to cite this article: Yongming Du, Yichao Hu, Mengmeng Qiu, Yuehua Sheng. Necroptosis-related gene to construct a signature to predict the prognosis and immune features in patients with cervical cancer. European Journal of Gynaecological Oncology. 2024; 45(6): 48-66. doi: 10.22514/ejgo.2024.116.